WRDC-TR-90-2028


# INVESTIGATION OF A TAPERED ARTERY MICRO HEAT PIPE FOR COOLING CERAMIC CHIP CARRIERS



G. P. Peterson and D. Wu
Department of Mechanical Engineering
Texas A&M University
College Station, TX 77843

January 1990

Final Report for Period January 1989 - February 1990



AERO PROPULSION AND POWER LABORATORY
WRIGHT RESEARCH AND DEVELOPMENT CENTER
AIR FORCE SYSTEMS COMMAND
WRIGHT-PATTERSON AIR FORCE BASE, OHIO 45433-6563

# NOTICE

WHEN GOVERNMENT DRAWINGS, SPECIFICATIONS, OR OTHER DATA ARE USED FOR ANY PURPOSE OTHER THAN IN CONNECTION WITH A DEFINITELY GOVERNMENT-RELATED PROCUREMENT, THE UNITED STATES GOVERNMENT INCURS NO RESPONSIBILITY OR ANY OBLIGATION WHATSOEVER. THE FACT THAT THE GOVERNMENT MAY HAVE FORMULATED OR IN ANY WAY SUPPLIED THE SAID DRAWINGS, SPECIFICATIONS, OR OTHER DATA, IS NOT TO BE REGARDED BY IMPLICATION, OR OTHERWISE IN any MANNER CONSTRUED, AS LICENSING THE HOLDER, OR ANY OTHER PERSON OR CORPORATION; OR AS CONVEYING ANY RIGHTS OR PERMISSION TO MANUFACTURE, USE, OR SELL ANY PATENTED INVENTION THAT MAY IN ANY WAY BE RELATED THERETO.

THIS REPORT HAS BEEN REVIEWED BY THE OFFICE OF PUBLIC AFFAIRS (ASD/PA) AND IS RELEASABLE TO THE NATIONAL TECHNICAL INFORMATION SERVICE (NTIS). AT NTIS IT WILL BE AVAILABLE TO THE GENERAL PUBLIC INCLUDING FOREIGN NATIONS.

THIS TECHNICAL REPORT HAS BEEN REVIEWED AND IS APPROVED FOR PUBLICATION.

Won S. Chang

WON S. CHANG
Project Engineer

Jerry E. Beam

JERRY E. BEAM, TAM
Power Technology Branch
Aerospace Power Division
Aero Propulsion and Power Laboratory

FOR THE COMMANDER

Michael D. Braydich

MICHAEL D. BRAYDICH, Maj, USAF
Actg Chief, Aerospace Power Division
Aero Propulsion & Power Laboratory

IF YOUR ADDRESS HAS CHANGED, IF YOU WISH TO BE REMOVED FROM OUR MAILING LIST, OR IF THE ADDRESSEE IS NO LONGER EMPLOYED BY YOUR ORGANIZATION PLEASE NOTIFY WRDC/POOS-3, WRIGHT-PATTERSON AFB, OH 45433-6563 TO HELP MAINTAIN A CURRENT MAILING LIST.

COPIES OF THIS REPORT SHOULD NOT BE RETURNED UNLESS RETURN IS REQUIRED BY SECURITY CONSIDERATIONS, CONTRACTUAL OBLIGATIONS, OR NOTICE ON A SPECIFIC DOCUMENT.

# REPORT DOCUMENTATION PAGE

| | |
|---|---|
| 1a. REPORT SECURITY CLASSIFICATION<br>Unclassified | 1b. RESTRICTIVE MARKINGS<br>None |
| 2a. SECURITY CLASSIFICATION AUTHORITY | 3. DISTRIBUTION / AVAILABILITY OF REPORT<br>Approved for Public Release<br>Distribution is unlimited |
| 2b. DECLASSIFICATION / DOWNGRADING SCHEDULE | |
| 4. PERFORMING ORGANIZATION REPORT NUMBER(S)<br>32526-5994 | 5. MONITORING ORGANIZATION REPORT NUMBER(S)<br>WRDC-TR- 90-2028 |
| 6a. NAME OF PERFORMING ORGANIZATION<br>Texas A&M University<br>6b. OFFICE SYMBOL (*If applicable*)<br>TAMU | 7a. NAME OF MONITORING ORGANIZATION<br>Aero Propulsion and Power Laboratory (WRDC/POOS)<br>Wright Research & Development Center |
| 6c. ADDRESS (*City, State, and ZIP Code*)<br>Department of Mechanical Engineering<br>Texas A&M University<br>College Station, Texas 77843 | 7b. ADDRESS (*City, State, and ZIP Code*)<br>Wright-Patterson AFB, Ohio 45433-6563 |
| 8a. NAME OF FUNDING / SPONSORING ORGANIZATION<br>Aero Propulsion & Power Lab<br>8b. OFFICE SYMBOL (*If applicable*)<br>WRDC/POOS | 9. PROCUREMENT INSTRUMENT IDENTIFICATION NUMBER<br>F33615-86-C-2723 |
| 8c. ADDRESS (*City, State, and ZIP Code*)<br>Wright-Patterson AFB, Ohio, 45433-6563 | 10. SOURCE OF FUNDING NUMBERS<br>PROGRAM ELEMENT NO. 63224C; PROJECT NO. L210; TASK NO. 00; WORK UNIT ACCESSION NO 26 |

11. TITLE (*Include Security Classification*)
Investigation of a Tapered Micro Heat Pipe for Cooling Ceramic Chip Carriers

12. PERSONAL AUTHOR(S)
G. P. Peterson and D. Wu

| 13a. TYPE OF REPORT | 13b. TIME COVERED | 14. DATE OF REPORT (*Year, Month, Day*) | 15. PAGE COUNT |
|---|---|---|---|
| Final | FROM 1/89 TO 2/90 | 1990, April, 30 | 36 |

16. SUPPLEMENTARY NOTATION

| 17. COSATI CODES | | | 18. SUBJECT TERMS (*Continue on reverse if necessary and identify by block number*) |
|---|---|---|---|
| FIELD | GROUP | SUB-GROUP | Heat Pipes, Micro, Miniature, Modeling Testing |
| | | | |
| | | | |

19. ABSTRACT (*Continue on reverse if necessary and identify by block number*)

In a previously sponsored project, a combined numerical and experimental investigation of several trapezoidal micro heat pipes was conducted. Although the resulting models were shown to accurately predict the steady-state performance limitations and operational characteristics, no experimental data on the transient operation were obtained. For this reason, an additional phase of the project was undertaken. This follow-on investigation included several major tasks including the expansion of the existing analytical model to predict transient performance, determine the effect of variations in the size, and optimize the cross-sectional shape. In addition, several micro heat pipes which utilized this optimized shape were evaluated experimentally to determine their suitability for removing heat from a ceramic chip carrier.

The result of this investigation was an experimentally verified transient numerical model capable of predicting the onset of dryout in a tapered micro (over)

| | |
|---|---|
| 20. DISTRIBUTION / AVAILABILITY OF ABSTRACT<br>☒ UNCLASSIFIED/UNLIMITED ☐ SAME AS RPT ☐ DTIC USERS | 21. ABSTRACT SECURITY CLASSIFICATION<br>Unclassified |
| 22a. NAME OF RESPONSIBLE INDIVIDUAL<br>W. S. Chang | 22b. TELEPHONE (*Include Area Code*)<br>(513) 255-6241<br>22c. OFFICE SYMBOL<br>WRDC/POOS |

19. cont'd

heat pipe during startup or variations in the evaporator thermal load was developed. Comparison of the numerical and experimental results indicate that the numerical model is capable of accurately predicting the maximum transport capacity prior to the onset of dryout, the temperature distribution throughout the longitudinal position, and the temperature difference between different locations on the heat pipe to within 0.3°C prior to the onset of dryout. In addition, the transient model was found to be capable of predicting the operation and temperature distribution of the tapered micro heat pipe to within ±12 % over a wide range of powers and operating temperatures.

As a result of this effort, the numerical model can be utilized to identify, evaluate, and better understand the phenomena that govern the transient behavior of micro heat pipes as a function of the physical shape, the properties of the working fluid, and the principal dimensions.

## TABLE OF CONTENTS

## NOMENCLATURE

| | |
|---|---|
| A | Cross-sectional area |
| d | Distance |
| $C_p$ | Specific heat |
| j | Evaporation |
| m | Mass flowrate |
| M | Molecular weight |
| P | Pressure |
| Q | Heat transfer |
| R | Universal gas constant |
| r | Radius of curvature |
| t | Time |
| T | Temperature |
| V | Velocity |
| W | Wetted perimeter |
| x | Length or distance |
| y | Distance |

Greek Alphabet:

| | |
|---|---|
| $\beta$ | Dimensionless parameter (Fig. 2) |
| $\theta$ | Wetting angle |
| $\mu$ | Viscosity |
| $\lambda$ | Latent heat |
| $\rho$ | Density |
| $\sigma$ | Surface tension |

Subscripts:

| | |
|---|---|
| a | Adiabatic |
| b | Boundary |
| c | Capillary, curvature |
| d | Diagonal |
| e | Evaporator |
| ec | Evaporation-condensation |
| f | Friction |
| h | Hydraulic |
| l | Liquid |
| m | Momentum, mean |
| o | Outer |
| p | Pipe |
| s | Solid |
| v | Vapor, viscous |

## 1.0 INTRODUCTION

The need to develop microelectronic devices capable of operating at increased performance levels with high reliability, requires better methods of thermal control.[1] With the recent trend towards increased miniaturization and component density, the thermal management problem increases dramatically. This is particularly true in the microelectronic components proposed for use in spacecraft applications where the physical space is at a premium, and the size of the heat removal system is a major contributor in the determination of overall spacecraft size.

In 1984, Cotter[2] described very small, miniature heat pipes for cooling microelectronic devices. He defined a micro heat pipe as "one so small that the mean curvature of the vapor-liquid interface is necessarily comparable in magnitude to the reciprocal of the hydraulic radius of the total flow channel." In practical terms, a micro heat pipe is a wickless, noncircular channel with an approximate diameter of 100-1000 μm and a length of about 10-20 mm. These micro heat pipes do not have a wick but use the mean curvature of the channel to pump the liquid from the condenser to the evaporator. In addition to the difficulties associated with the manufacturing, cleaning, and filling of these devices, they are very sensitive to the shape, size, and amount of working fluid present. Since the liquid-vapor interface changes continually along the pipe, care must be exercised to ensure proper wetted conditions without flooding.

Under a previous contract with Wright-Patterson AFB, steady-state experimental and analytical investigations of a trapezoidal micro heat pipe were conducted to identify and better understand the phenomena which govern the performance limitations and operating characteristics. The analytical portion of the investigation began with the development of a steady-state model, in which the effects of the extremely small characteristic dimensions on the

conventional steady-state heat pipe modeling techniques were examined.

In addition to the modeling portion of the investigation, several micro heat pipes approximately 1 $mm^2$ in cross-sectional area and 57 to 60 mm in length, were evaluated experimentally to determine the accuracy of the model and provide verification of the micro heat pipe concept. Tests were conducted in a vacuum environment to eliminate conduction and convection losses. The steady-state experimental results obtained were compared with the analytical and numerical models and verified the modeling predictions for both the steady-state model and the transient model at steady-state. The results indicated that the wetting angle was the single most important factor contributing to the tranaport capacity and thermal behavior of these types of heat pipes.

Micro heat pipes have a wide range of applications. Of particular interest here is the thermal control of discrete semiconductor devices. Other applications include the thermal control of infrared detectors and the cooling of the leading edges of hypersonic aircraft. Smaller micro heat pipes, (less than 0.05 $mm^2$ in cross-sectional area), could be incorporated into semiconductor devices as an integral part of the chip. This would provide a mechanism for eliminating the localized hot spots associated with semiconductor devices and significantly improve the chip reliability. In addition, these micro heat pipes could provide a method for collecting and dissipating the high thermal loads associated with the three-dimensional chip architectures being developed for use in fifth generation computers.[3]

### 1.1 Objectives of the Investigation

Although the models developed previously were shown to accurately predict the steady-state performance limitations and operational characteristics,[4] no experimental data on the transient operation and characteristics were obtained.

In addition, several factors which significantly affect both the steady-state and transient behavior required continued study. To further understand the behavior of these types of devices, a transient model was developed to predict the behavior during startup or variations in the evaporator thermal load.

This follow-on investigation included several major tasks. The first of these involved the expansion of the existing analytical model to include the capability of accurately predicting the transient performance of micro heat pipes. Second, was a determination of the effect of variations in the cross-sectional shape of the device and the optimization of this shape. Third, was the experimental investigation of a micro heat pipe which utilized this optimum shape to remove heat from a ceramic chip carrier. And finally, was a comparision of the analytical predictions and the experimental results.

The following report is divided into two major sections: the first deals with a description of the development and expansion of the transient numerical model, while the second describes the experimental program and compares the modeling predictions and the experimental results.

## 2.0 DESCRIPTION OF THE NUMERICAL MODEL

Babin et al.[4] described a micro heat pipe as one which satisfies the condition

$$\frac{r_c}{r_h} \geq 1 \qquad (1)$$

where $r_c$ is the capillary radius of the heat pipe and $r_h$ is the hydraulic radius of the flow channel. In these, as in conventional heat pipes, the high thermal conductivity is the result of the evaporation and condensation process occurring within the heat pipe.[5,6] For this reason, determination of the evaporation and condensation rate of the liquid plays a key role in evaluating the thermal

characteristics and heat transport limitations of these heat pipes. In the present model, an expression for the molecular flux of evaporation, j, presented by Collier[7] and later used by Colwell and Chang[8] was employed. This relationship is

$$j = \left(\frac{M}{2\pi RT}\right)^{.5} (P_s - P_v) \tag{2}$$

where M is the molecular weight of the fluid, R is the universal gas constant, T is the absolute temperature, $P_s$ is the saturation pressure, and $P_v$ is vapor pressure. When $P_s$ is greater than $P_v$, j is positive and the liquid evaporates. When $P_s$ is less than $P_v$, j is negative and the vapor condenses. In the development of the numerical model presented here, the evaporation-condensation rate was assumed to be proportional to the liquid-vapor interface area in each section of the heat pipe, i.e.

$$\Delta M_{ec} = j\ \Delta A_e = jW_{ec}\Delta x \tag{3}$$

where $\Delta A_{ec}$ is the evaporation-condensation surface area in one section, $W_{ec}$ was the perimeter of the liquid-vapor interface, and $\Delta x$ is the section length.

For a given latent heat, $\lambda$, the rate of the heat released or absorbed in any section can be determined from:

$$\Delta Q_{ec} = \lambda \Delta M_{ec} \tag{4}$$

In order for a heat pipe to operate properly, the capillary pressure must be sufficient to overcome the difference of the liquid and vapor pressures, or

$$P_{vl} = P_v - P_l = \sigma / r_c \tag{5}$$

where, $P_v$ is the vapor pressure, $\sigma$ is the liquid surface tension and $r_c$ is the radius of curvature of the liquid-vapor interface. Since both $P_{vl}$ and $r_c$ are functions of the axial position, the derivative of the above equation yields:

$$\frac{dP_{vl}}{dx} = \frac{-\sigma}{r_c^2} \frac{dr_c}{dx} \quad . \tag{6}$$

Expressing this over a finite interval yields

$$\Delta P_{vl} = \frac{-\sigma}{r_c^2} \Delta r_c \tag{7}$$

where

$$\Delta P_{vl} = \Delta P_{fv} + \Delta P_{mv} + \Delta P_{fl} + \Delta P_{ml} + \Delta P_g. \tag{8}$$

The pressure changes are those due to the liquid and vapor friction and the momentum changes are those occurring in any one section along the heat pipe.

Based on the momentum equation, the pressure drops due to friction for laminar flow can be expressed as:

$$\Delta P_f = \frac{2\mu \Delta x V}{r_h^2} \tag{9}$$

where $\mu$ is the viscosity of the fluid, $r_h$ is the hydraulic radius, and V is the velocity of the flow which is equal to a function of the mass flow rate, the density, and the area.

The total pressure drop due to the momentum change can be expressed as:

$$\Delta P_m = \frac{V\dot{\Delta m} + \dot{m}\Delta V + \dot{\Delta m}\Delta V}{A} \quad . \tag{10}$$

The energy equation used in this model can be written as

$$Q_{in} = Q_{out} + Q_r \tag{11}$$

where

$$Q_r = \int \rho_l A_l C_{Pl} \Delta T_l dx + \int \rho_v A_v C_{Pv} \Delta T_v dx + \int \rho_s A_s C_{Ps} \Delta T_s dx \tag{12}$$

$C_{Pl}$, $C_{Pv}$ and $C_{Ps}$ are the heat capacities of the liquid, vapor and solid

boundaries respectively and the $\Delta T$'s are the corresponding temperature changes.

The continuity equation can be written as

$$\int \rho_v A_v \, dx + \int \rho_l A_l \, dx = \text{constant} = \text{fluid charge} \tag{13}$$

and the total volume inside the heat pipe can be defined and expressed as:

$$Vol = Vol_l + Vol_v \tag{14a}$$

and

$$A = A_l + A_v \tag{14b}$$

respectively.

As is the case for larger heat pipes, micro heat pipes consist of three basic sections, an evaporator and a condenser, separated by an adiabatic section. Each of these sections has a different set of boundary conditions, and as a result, have been treated independently.

## 2.1 Evaporator Region

The single boundary condition utilized in the evaporator section is the time dependent heat flux. For a specific input heat flux, the saturation pressure at a given location can be obtained by using a combination of the molecular flux expression given in Eq. (2) and the energy conservation equation given in Eq. (12). Assuming that a temperature change at the boundary yields a corresponding temperature change of the liquid, these equations take the following form:

$$P_s = \frac{\Delta Q_{ec}}{(M/2\pi RT_l)^{1/2} \, \Delta x W_{ec}} + P_v \tag{15}$$

$$\Delta Q_l = \frac{C_{Pl} \rho_l A_l \Delta x \Delta T_l}{\Delta t} \tag{16}$$

$$\Delta Q_s = \frac{C_{Ps} \rho_s A_s \Delta x \Delta T_s}{\Delta t} \tag{17}$$

$$\Delta Q_{in} = \Delta Q_{ec} + \Delta Q_l + \Delta Q_s \tag{18}$$

Since $T_l$ is a function of $P_s$, Eqs. 15 through 18 are coupled and can be solved using an iterative method with relaxation to obtain values for $T_l$, $\Delta Q_{ec}$, $\Delta Q_l$, and $\Delta Q_s$. Because the difference between the boundary and liquid temperatures, $\Delta T_{bl}$, is proportional to the input heat flux, the boundary temperature can be obtained by adding $\Delta T_{bl}$ to $T_l$.

## 2.2 Adiabatic Region

In the adiabatic section, the latent heat absorbed by evaporation and given up by condensation is equal to the sensible heat absorbed or rejected by the liquid and/or the heat pipe case. The governing equations for this section can therefore be expressed as:

$$\Delta Q_{ec} = \lambda W_{ec} \Delta x \left( \frac{M}{2\pi R T_l} \right)^{1/2} (P_s - P_v) \tag{19}$$

$$\Delta Q_l = \frac{C_{Pl} \rho_l A_l \Delta T_l \Delta x}{\Delta t} \tag{20}$$

$$\Delta Q_s = \frac{C_{Ps} \rho_s A_s \Delta T_b \Delta x}{\Delta t} \tag{21}$$

$$\Delta Q_{ec} + \Delta Q_l + \Delta Q_s = 0 \, . \tag{22}$$

By assuming no temperature drop at the liquid/case boundary, i.e., $T_l = T_b$, Eqs. (19-22) can also be solved using an iterative technique to obtain $\Delta Q_{ec}$, $\Delta Q_l$, $\Delta Q_s$, and $\Delta T_l$.

## 2.3 Condenser Region

In the condenser region, the boundary temperature of the heat pipe was assumed to be constant, resulting in governing equations similar to those used in the adiabatic section,

$$\Delta Q_{ec} = \lambda W_{ec} \Delta x \left( \frac{M}{2\pi R T_l} \right)^{1/2} (P_s - P_v) \tag{23}$$

$$\Delta Q_l = \frac{C_{Pl} \rho_l A_l \Delta T_l \Delta x}{\Delta t} \tag{24}$$

$$\Delta Q_s = \frac{C_{Ps} \rho_s A_s \Delta T_b \Delta x}{\Delta t} \tag{25}$$

$$\Delta Q_{ec} + \Delta Q_l + \Delta Q_s = Q_{out} \tag{26}$$

Although in normal operation, the condenser boundary temperature would vary with the input power, in a controlled laboratory experiment this condition is easily obtained by controlling the temperature and/or flowrate of the condenser coolant.

## 2.4 General Assembly

Because the evaporation-condensation rate is extremely sensitive to changes in the vapor pressure, a predictor-corrector treatment was applied to obtain a stable solution. Initially, the evaporation rate was assumed to be equal to the condensation rate and the vapor pressure was calculated. This vapor pressure was then used to compute the change in the mass of vapor and hence, the difference between evaporation and condensation. The original assumption of equal evaporation and condensation rates was then checked and the values updated. Preliminary tests indicated that the solution was stable regardless of the time step size used. In comparison, prior to using this predictor-corrector treatment, the solution vibrated with increasing magnitude for time step sizes below 0.01 millisecond.

The solution procedure consisted of initializing the variables and arrays, and by iteration, computing the boundary, liquid, and vapor temperatures along with the evaporation and condensation rates, the pressure drops, and the

flowrates, for each section. The resulting radii of curvature for the liquid-vapor interface was then computed and the liquid-vapor mass flowrate corrected using the resulting vapor pressure.

## 2.5 Transient Modeling Results

Using the previously described model, the cross-sectional shape and size of a micro heat pipe designed for applications involving the thermal control of ceramic chip carriers were optimized. Figure 1 illustrates this application and the general heat pipe configuration. Figure 2 illustrates the critical cross-sectional dimensions and shape. An interative approach was utilized to develop the optimum shape. Once this had been accomplished, a free surface energy minimization technique[10] was used to determine the stable cross-sectional liquid configuration. Results of this analysis indicated that regardless of the orientation of the heat pipe, the majority of the liquid was contained in the upper corners (acute angle) as shown in Fig. 2, and that only a very small fraction was contained in the lower corner regions.

Once the optimum shape had been determined, the numerical model was used to predict the axial temperature distribution of the heat pipe for a given operating condition. Figure 3 illustrates the axial temperature distribution for an input power of 0.18 W. The temperature in the evaporator region shown on the left end decreases rapidly with a small continued decrease occurring in the adiabatic section and an almost constant temperature in the condenser section. Three temperatures are indicated: the boundary and liquid temperatures which are, because of their similarity, almost identical, and the base temperature. Although significant axial temperature differences exist in the boundary and liquid profiles, it is interesting to note that vapor temperature is almost constant throughout both the adiabatic and condenser regions.

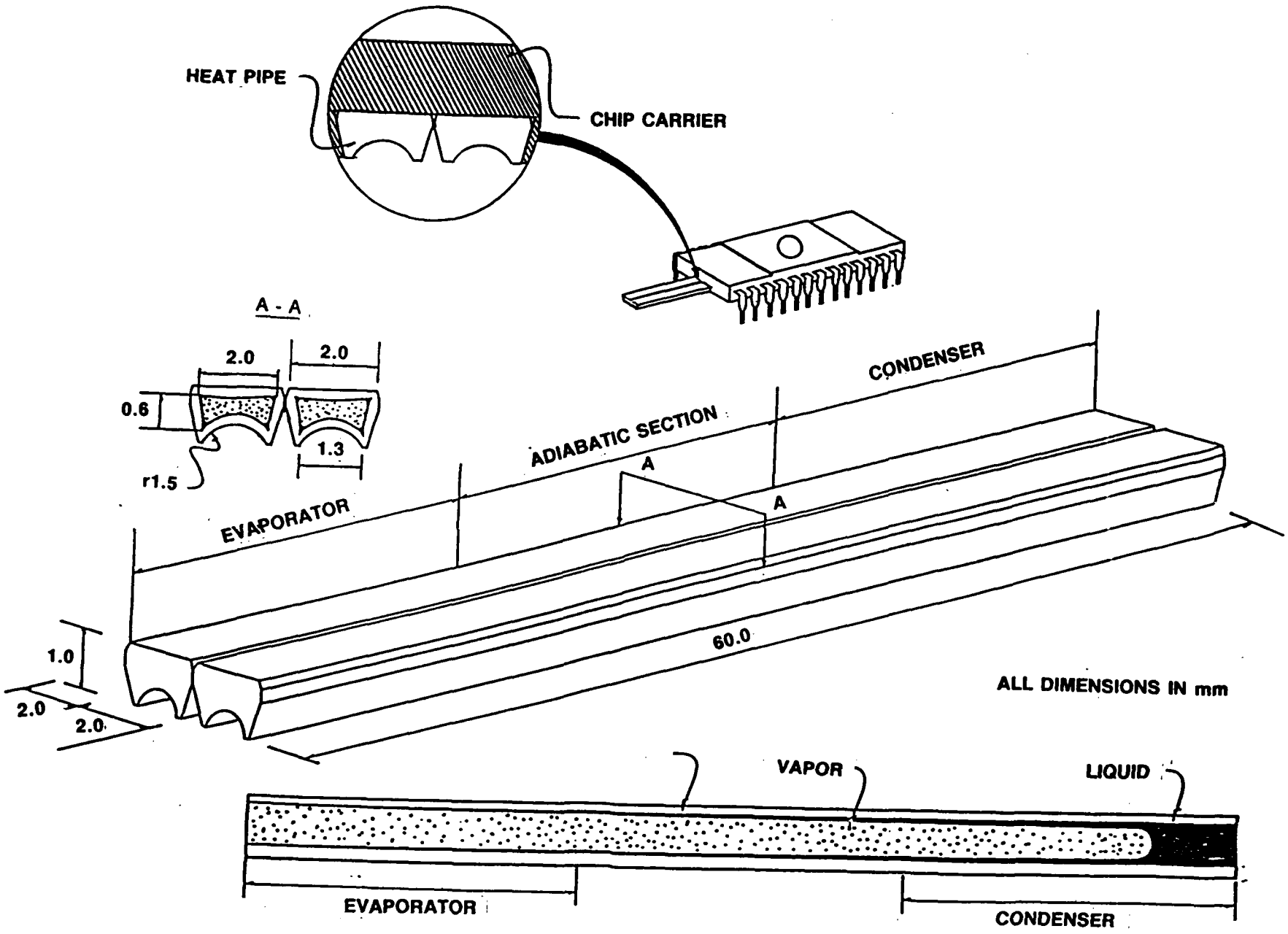


Fig. 1 Tapered micro heat pipe.

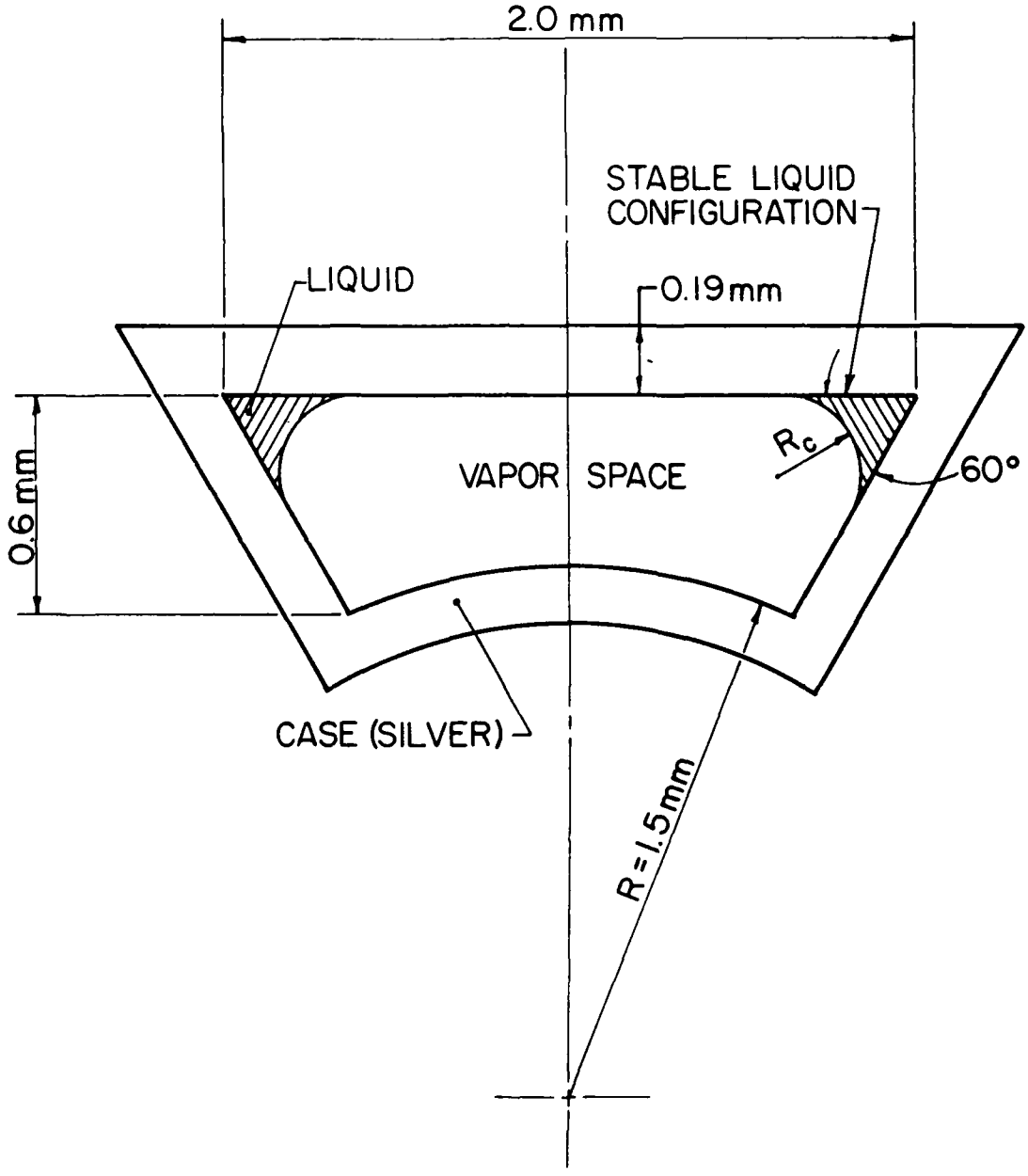


Fig. 2 Cross-sectional shape of the modeled heat pipe.

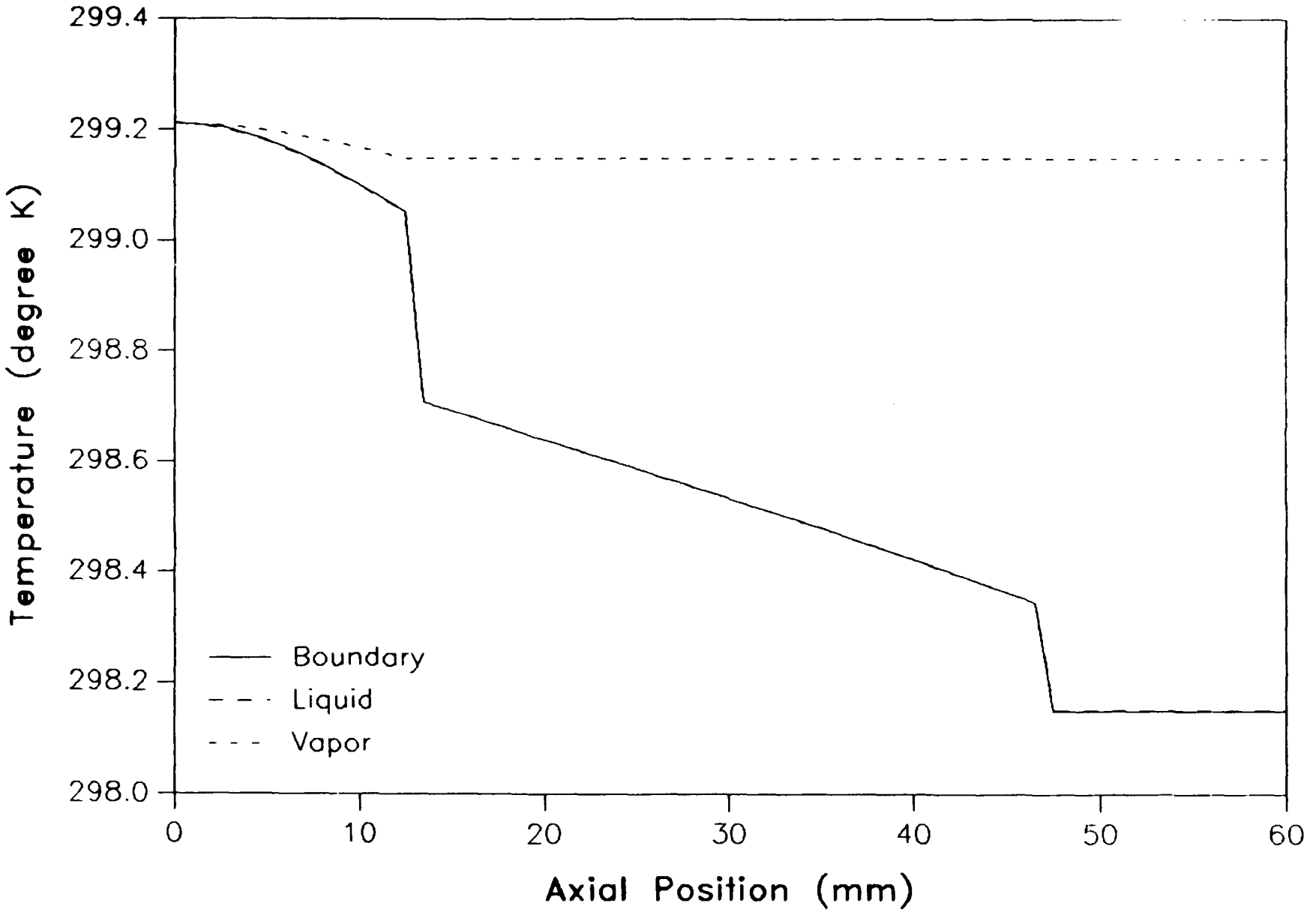


Fig. 3 Steady-state temperature distribution as predicted by the transient model.

Figure 4 illustrates the liquid mass flow rate as a function of time and axial position, as was the case for the previously analyzed trapezoidal heat pipe. The tapered micro heat pipe evaluated here displayed reverse liquid flow during startup. This reverse liquid flow is believed to be the result of an imbalance in the overall pressure drop. Because the evaporation rate does not provide a sufficient change in the liquid-vapor interfacial curvature adequate to compensate for the total pressure drop resulting from the temperature change, some liquid is forced from the evaporator region towards the condenser region through the corner regions of the heat pipe. Once the heat pipe reaches full power, the reverse liquid flow disappears, and the liquid mass flow rate gradually increases until a steady-state condition is reached and the liquid mass flow rate is equal to the vapor mass flow rate in any given section. This phenomena is more apparent in Fig. 5, which illustrates the pressure as a function of axial position for 10 second intervals approaching steady-state. As shown, 10 seconds after startup the pressure of both the liquid and vapor are higher in the evaporator and gradually decrease with position. This is the phenomena which promotes flow away from the evaporator and towards the condenser. Once steady-state has been achieved, the liquid pressure is much lower in the evaporator region and increases dramatically with position, promoting flow back towards the evaporator.

## 3.0 EXPERIMENTAL PROGRAM

To verify the accuracy of the transient model and determine the maximum heat transport capacity, further experimental investigations were conducted using a tapered micro heat pipe designed specifically for use in the thermal control of ceramic chip carriers. In the application illustrated in Fig. 1, this micro heat pipe fits securely under the chip and is attached to the chip carrier. 4

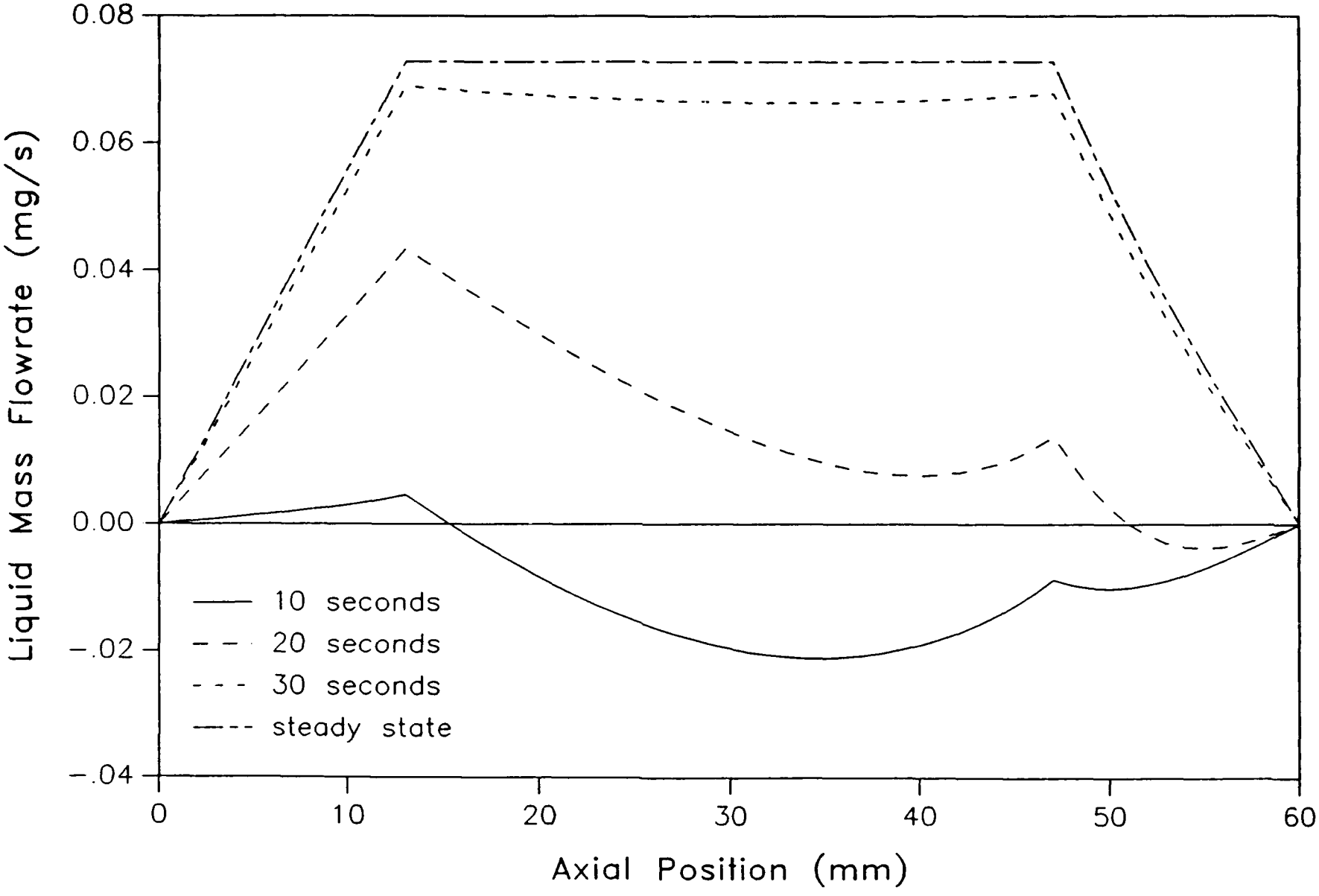


**Fig. 4 Liquid mass flow rate as a function of time and axial position.**

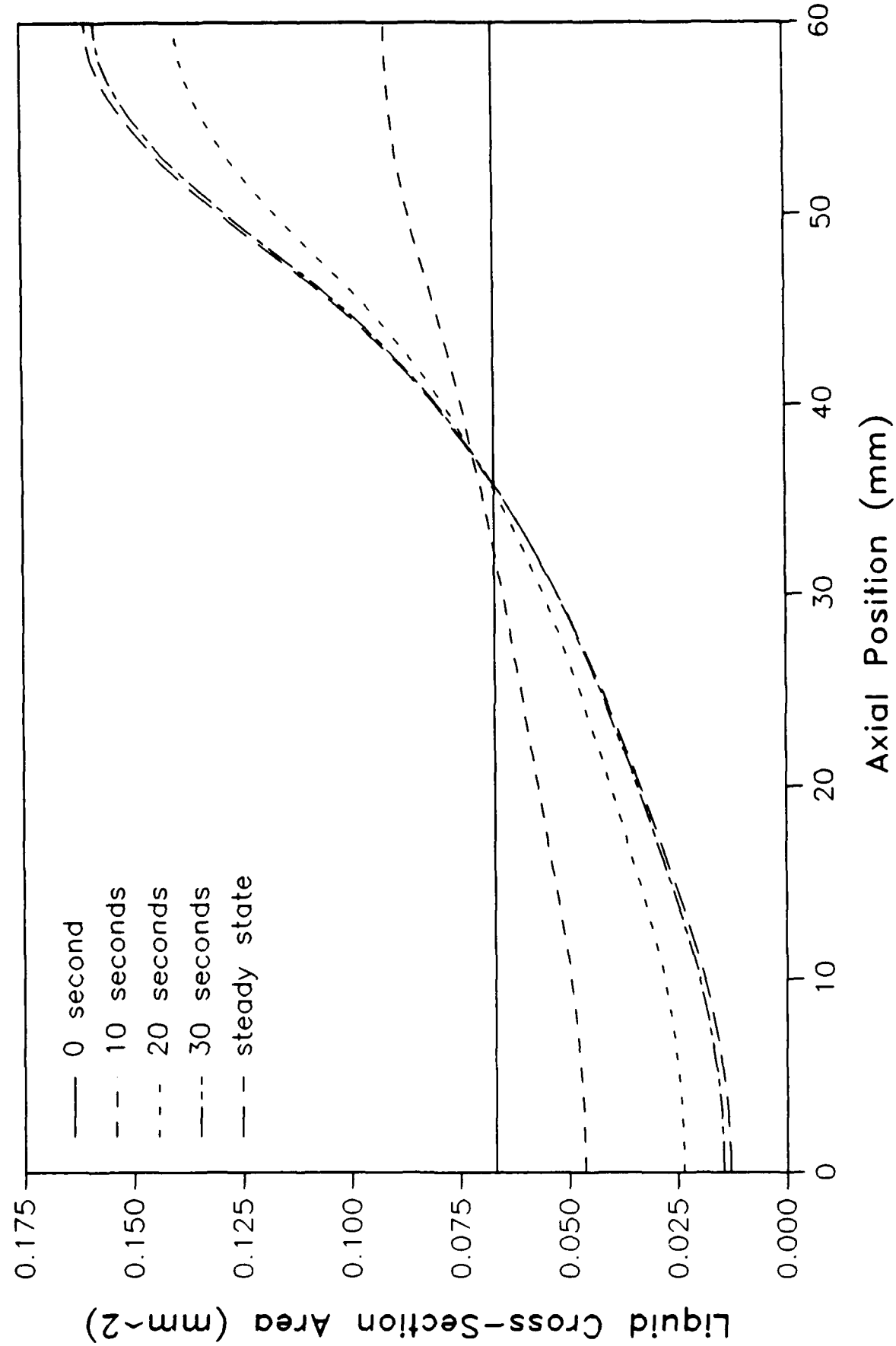


**Fig. 5 Liquid cross-sectional area as a function of time and axial position.**

Small fins located at the condenser end of the heat pipe promote the cooling of the condenser by free convection.

### 3.1 Experimental Test Facility

The experimental test facility used for this investigation has been previously described by Peterson et al.[9] Figure 6 illustrates the vacuum test facility while Fig. 7 illustrates the actual heat pipe test stand. Although the test facility and procedure were similar to the one used for the trapezoidal heat pipe, in the present investigation, the heat source used was a thin nichrome strip heater located only on the top portion of the heat pipe. Further, in addition to a series of eight copper-constantan thermocouples attached to the underside of each test pipe, three in the evaporator section, four in the adiabatic section, and one at the inlet to the condenser, an infrared thermal measurement system was used to monitor the temperature distribution in the heat pipe. A Hughes Probe Eye TVS model 3000 infrared camera in conjunction with an RGB monitor and a real time recorder were used to observe the test pipe during both startup and transient operation. Using this system the temperature distribution along the heat pipe could be measured with an accuracy of $\pm 0.05°C$. To reduce heat losses through convection, all of the tests were conducted in a vacuum of $< 10^{-2}$ Torr. The entire test facility was encased in a stainless steel vacuum chamber equipped with a single crystal silicon window which allowed observation with the infrared thermal measurement system. A mechanical roughing pump in series with an oil diffusion pump was used to obtain the required vacuum.

### 3.2 Experimental Procedure

In order to fully understand the operational characteristics and performance limitations of this tapered micro heat pipe, an experimental test plan was developed. This test plan was comprised of three principal tasks:

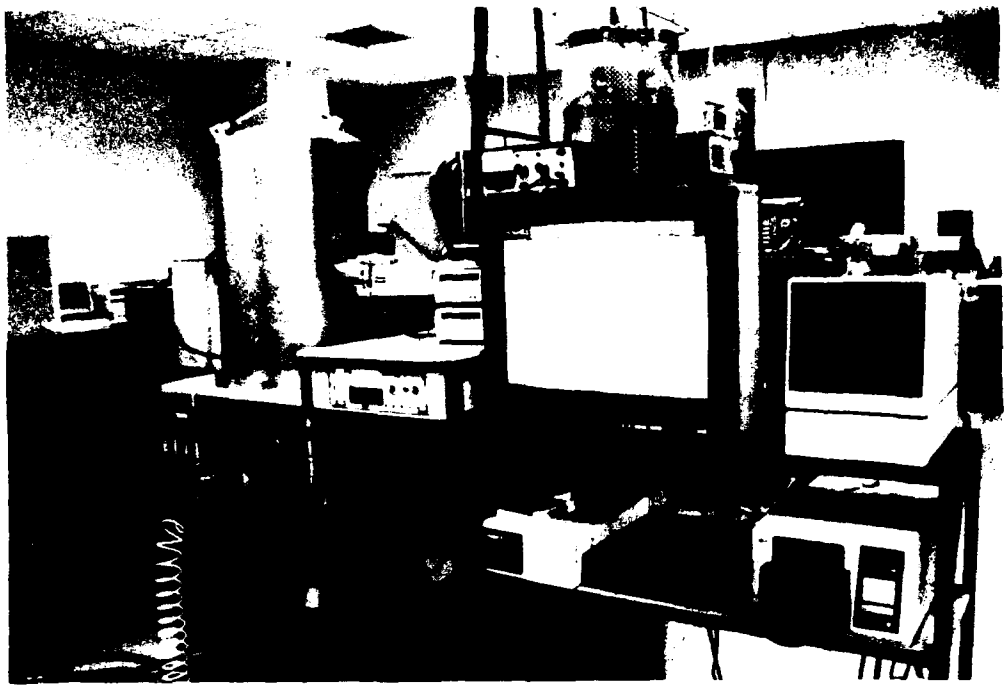

Fig. 6 Experimental Test Facility.

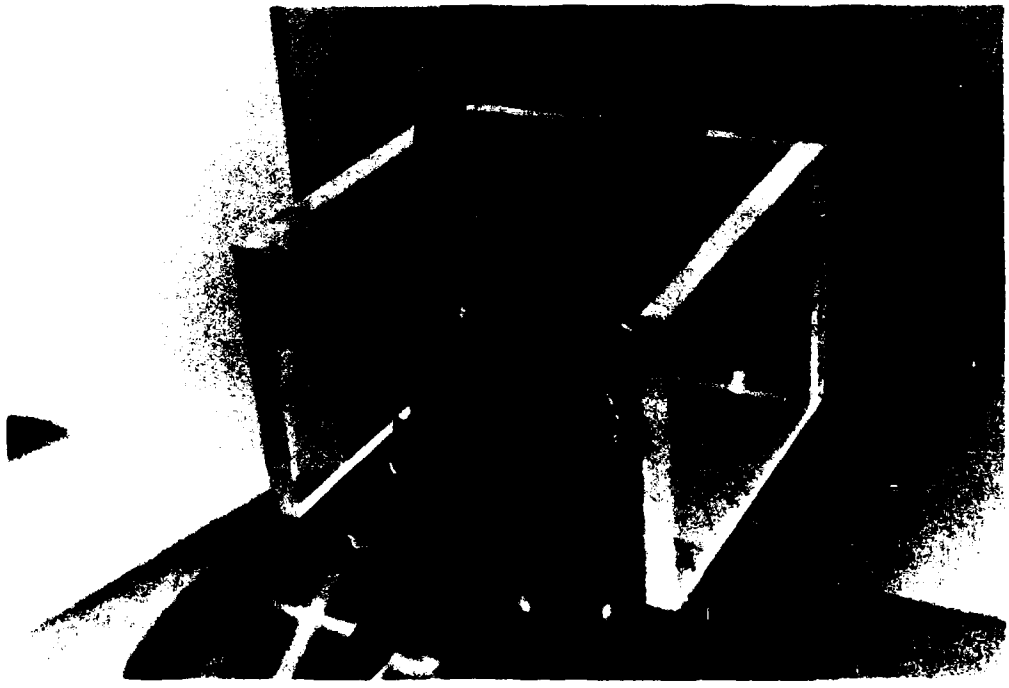

Fig. 7 Experimental Test Stand.

i. testing of a charged silver heat pipe to determine the transient characteristics.

ii. testing of a charged silver heat pipe to determine the steady-state behavior for different temperatures and tilt angles.

iii. testing of an uncharged silver heat pipe for comparison with the charged heat pipe results.

The heat pipe was first inserted into the cooling chamber with the condenser portion inside. Then a nichrome resistance heater was attached to the upper surface of the evaporator. Both the condenser and the evaporator portion were 1.27 cm in length with the remaining portion serving as the adiabatic region. The entire assembly was then mounted on the test fixture as previously described.[4] Once the desired vacuum has been obtained, the cooling bath temperature was adjusted and the power to the evaporator portion of the heat pipe was turned on, thermocouple measurements were taken at approximately 0.5 second intervals with temperature readings for each of the nine thermocouples recorded as a function of time. The heat input for the steady-state tests was increased in small increments, and adequate time was allowed for each incremental increase to allow the heat pipe to stabilize. Once the desired test condition had been reached, temperature measurements were taken for a period of several minutes to insure steady-state conditions. To obtain data for the next successive power level, the temperature of the cooling bath was adjusted to hold the temperature at the entrance to the condenser region constant.

## 3.3 Experimental Results

Figure 8 illustrates transient temperature characteristics of the tapered micro heat pipe for an input power of 0.508 W and a condenser temperature of 23°C. The abscissa is shown as a temperature difference between the thermocouple located at the inlet to the condenser and the one indicated in the legend. As illustrated, the heat pipe reaches a steady-state value very quickly

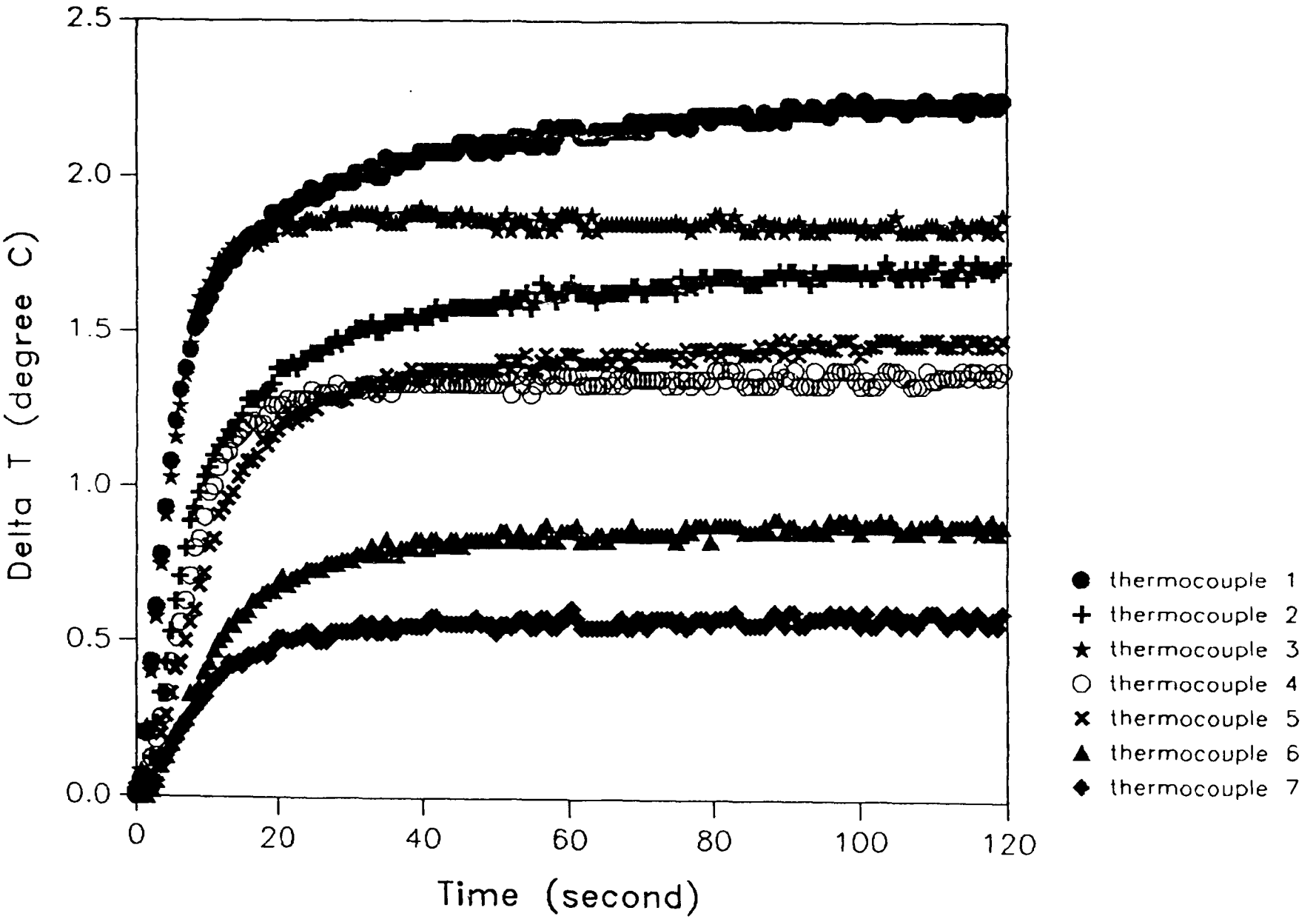


**Fig. 8 Transient temperature distribution (Power 0.058 W, $T_c$ 23°C).**

with approximately 90% of the maximum power obtained by approximately 20 seconds. At a time less than 20 seconds, Thermocouples 1 and 3 yield approximately identical readings. At 15 seconds, however, they begin to separate and the temperatures start to diverge. This rapid separation is believed to be the result of the onset of dryout. Note that both Thermocouples 1 and 3 are considerably hotter than Thermocouple 2. This may be due to the presence of the lead wires at each end of the heater but this justification was not verified. When there is no dryout of the corner regions, the temperature drops between Thermocouples 1 and 2, and 2 and 3, respectively, will be approximately equal.

Figure 9 illustrates the temperature difference between each of the thermocouples as a function of the power input. Again the abscissa is shown as a temperature difference between the thermocouple located at the inlet to the condenser and the one indicated in the legend. As illustrated, the heat pipe remains approximately isothermal along the entire length for powers between approximately 0.5 and 1.3 W. Prior to the power level of 0.5 W, a majority of the heat is either conducted axially through the wall of the heat pipe or radiated to the environment. At a value of 1.3 W, rapid increases in the evaporator temperature (as indicated by Thermocouples 1, 2, and 3) occur. These increases cascade throughout the evaporator indicating the dryout has begun and is progressing along the length. This is more apparent in Fig. 10, which illustrates the same experimental results; however, the axis has been enlarged to clarify the temperature differences. At approximately 2 W, this dryout has reached Thermocouple 4 located in the adiabatic section. This dryout "front" then proceeds reaching Thermocouple 5 at a power of approximately 3 W. It is interesting to note that at approximately 0.4 W, Thermocouples 3 and 4 invert as do Thermocouples 6 and 7 at a power of approximately 0.9 W. No explanation has

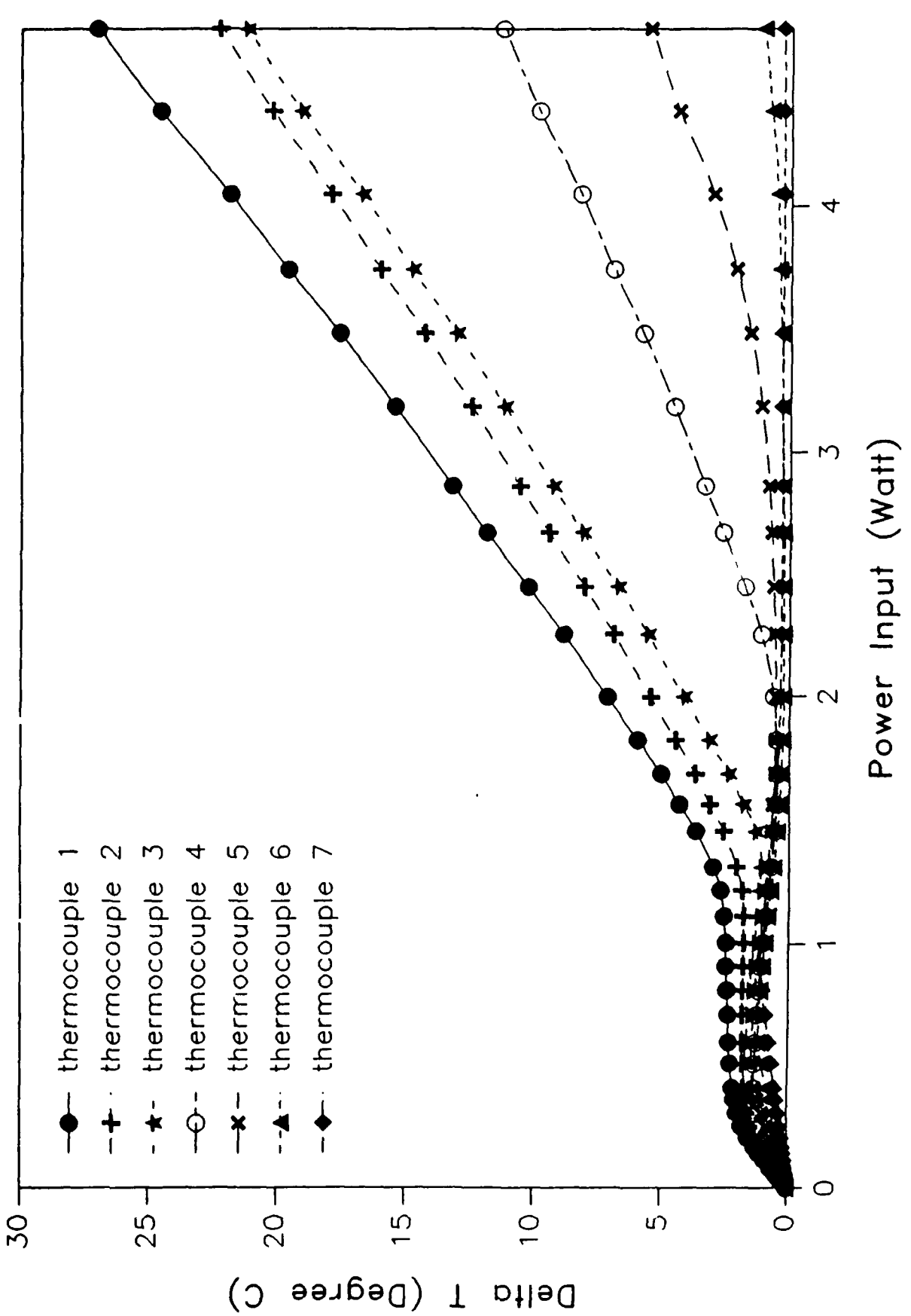


Fig. 9 Steady-state temperature distribution as a function of the input power (No tilt, $T_c$ 24.5°C).

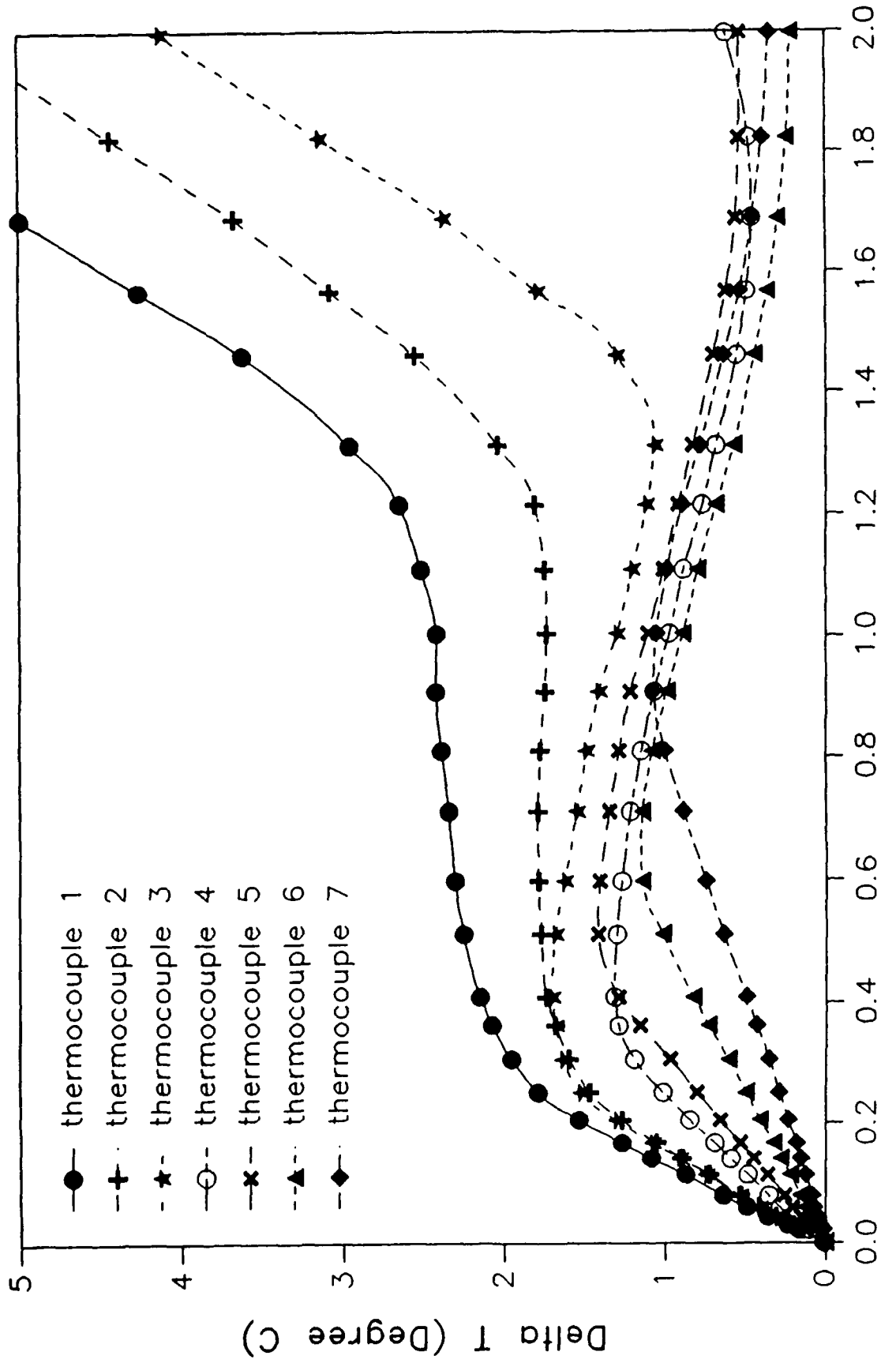


**Fig. 10 Enlarged steady-state temperature distribution as a function of the input power (No tilt, $T_c$ 24.5°C).**

been found to determine the cause of this phenomena, however, it was shown to be repeatable.

As mentioned previously, at power levels below 0.5 W, much of the heat is given off by radiation or conducted axially through the wall of the heat pipe. This is more clearly apparent in Fig. 11, which illustrates the experimental results for an uncharged heat pipe using the same condenser temperature and power levels used for the previous figures. As illustrated, the temperature difference indicated by the straight line, has the same slope for each of the corresponding thermocouples indicating that at these power levels, the axial temperature drop is the same for both the uncharged and charged heat pipes. However, as the power level increases, the heat pipe begins to operate more efficiently, and the axial temperature drop remains constant. This phenomena is similar to that observed in very short heat pipes. At low powers they are relatively inefficient owing to the thermal resistance of the case, wick, etc., but as the length increases, the advantages become clear.

To determine the effect of tilt angle on the operation of the tapered micro heat pipe, several tests were conducted with similar input powers, but at different tilt angles. Figure 12 illustrates the experimental results for the tapered heat pipe horizontal orientation at a power of 0.12 W and a condenser temperature of 25°C. Figure 13 shows an orientation 15 degrees with the horizontal (evaporator up), and Figure 14, at an orientation of 15 degrees from the horizontal with the evaporator down. As illustrated, the experimental results demonstrate very little difference in the temperature distribution along the pipe as a function of the input power because of tilt.

## 3.4 Comparison of Experimental and Analytical Results

Figure 15 compares the experimental data with the temperature distribution

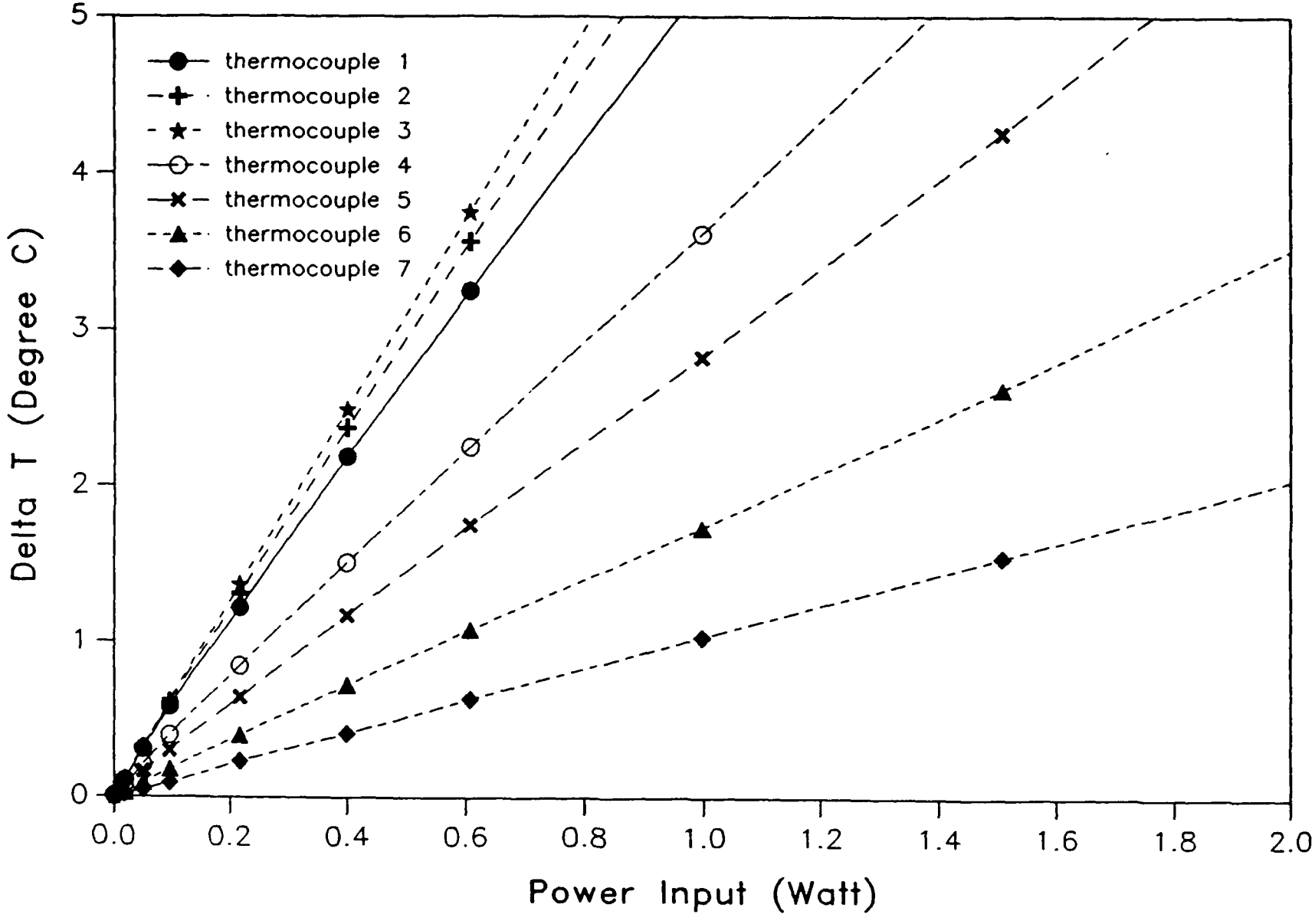


Fig. 11 Steady-state temperature distribution as a function of the input power for an uncharged heat pipe, ($T_c$ 24.5°C).

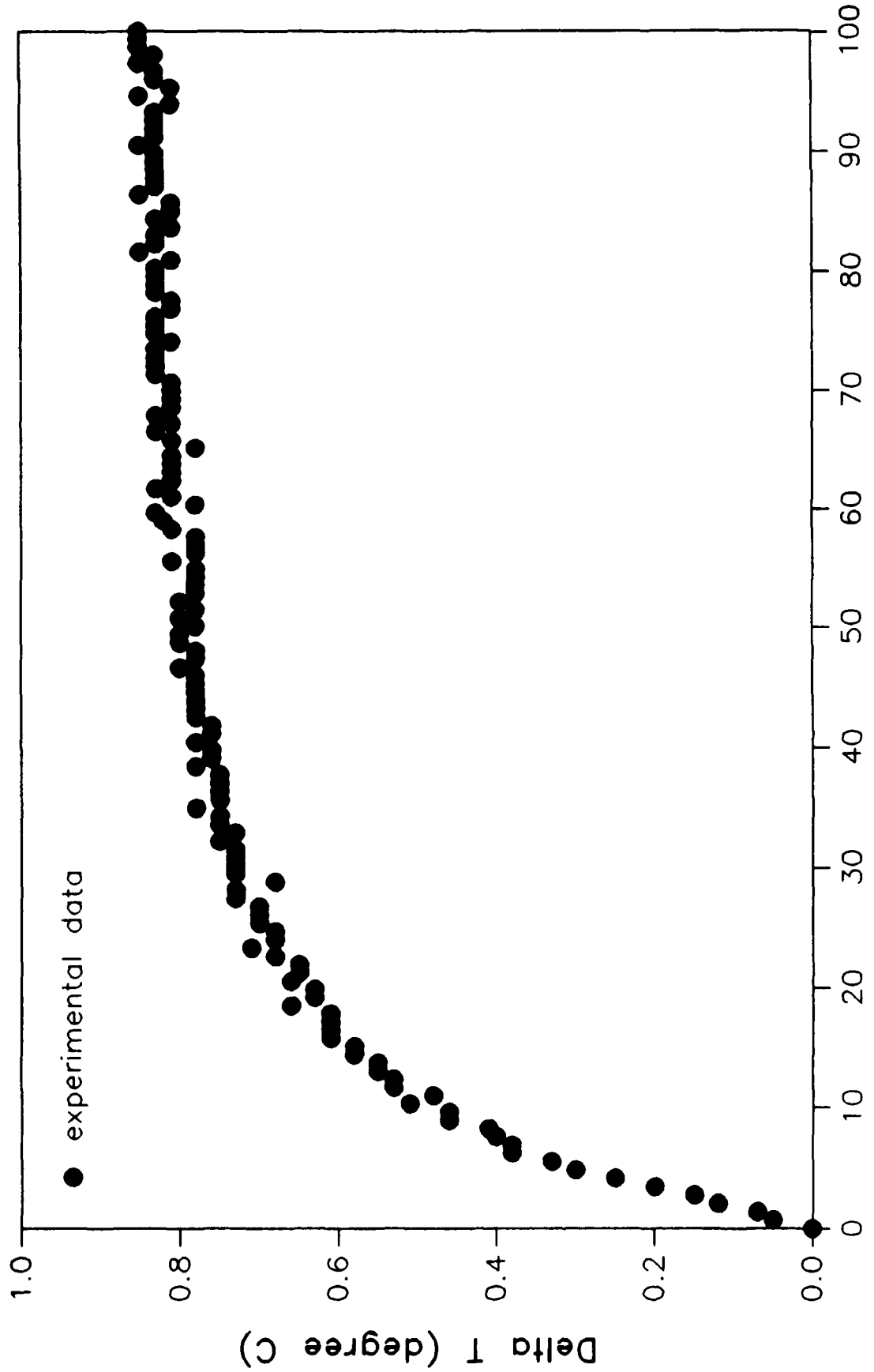


Fig. 12 Transient behavior prior to the onset of dryout, (Power 0.12 W, $T_c$ 24.5°C, no tilt).

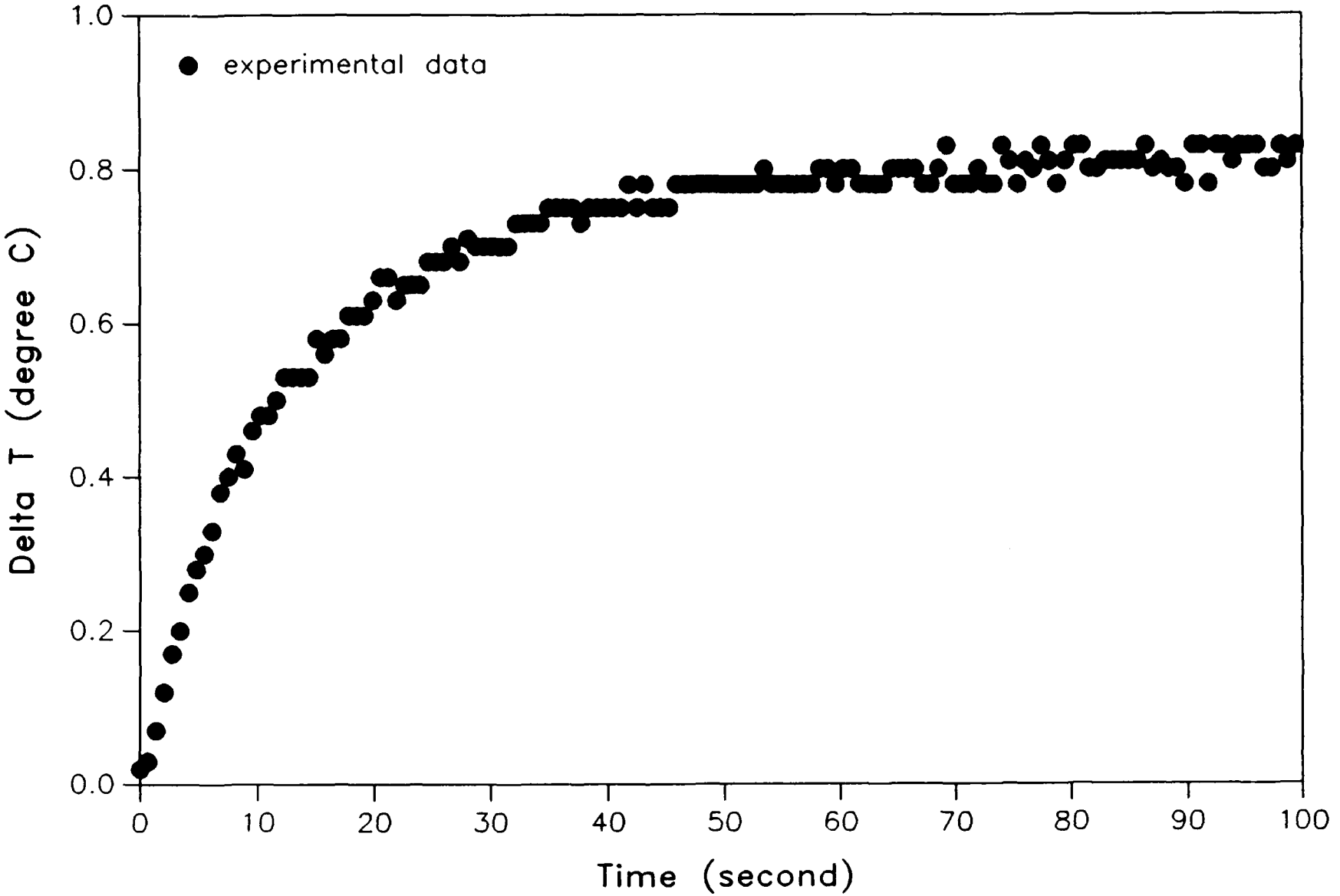


Fig. 13 Transient behavior prior to the onset of dryout, (Power 0.12 W, $T_c$ 24.5°C, 15 degree tilt evaporator up).

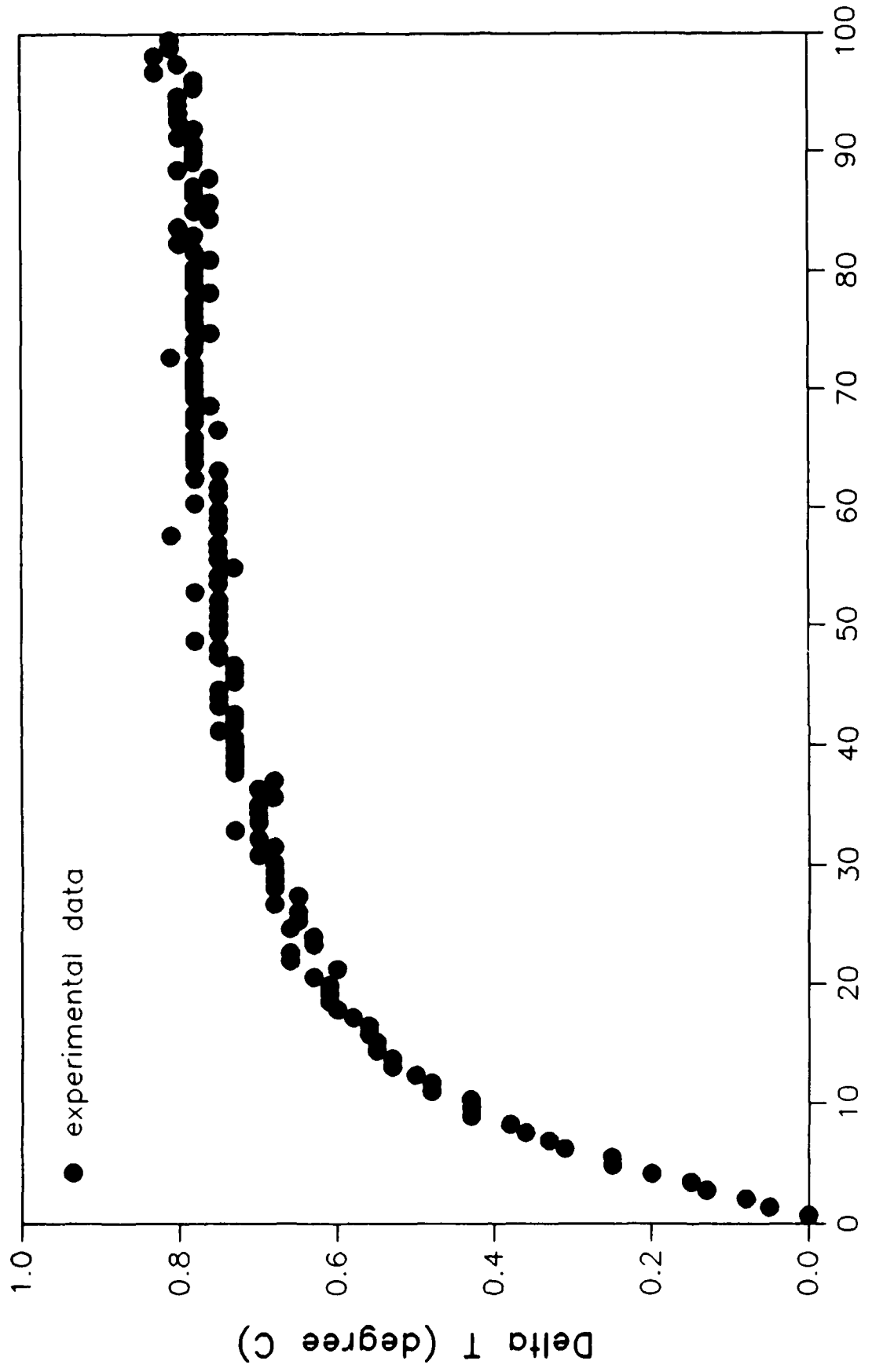


Fig. 14 Transient behavior prior to the onset of dryout, (Power 0.12 W, $T_c$ 24.5°C, 15 degree tilt evaporator down).

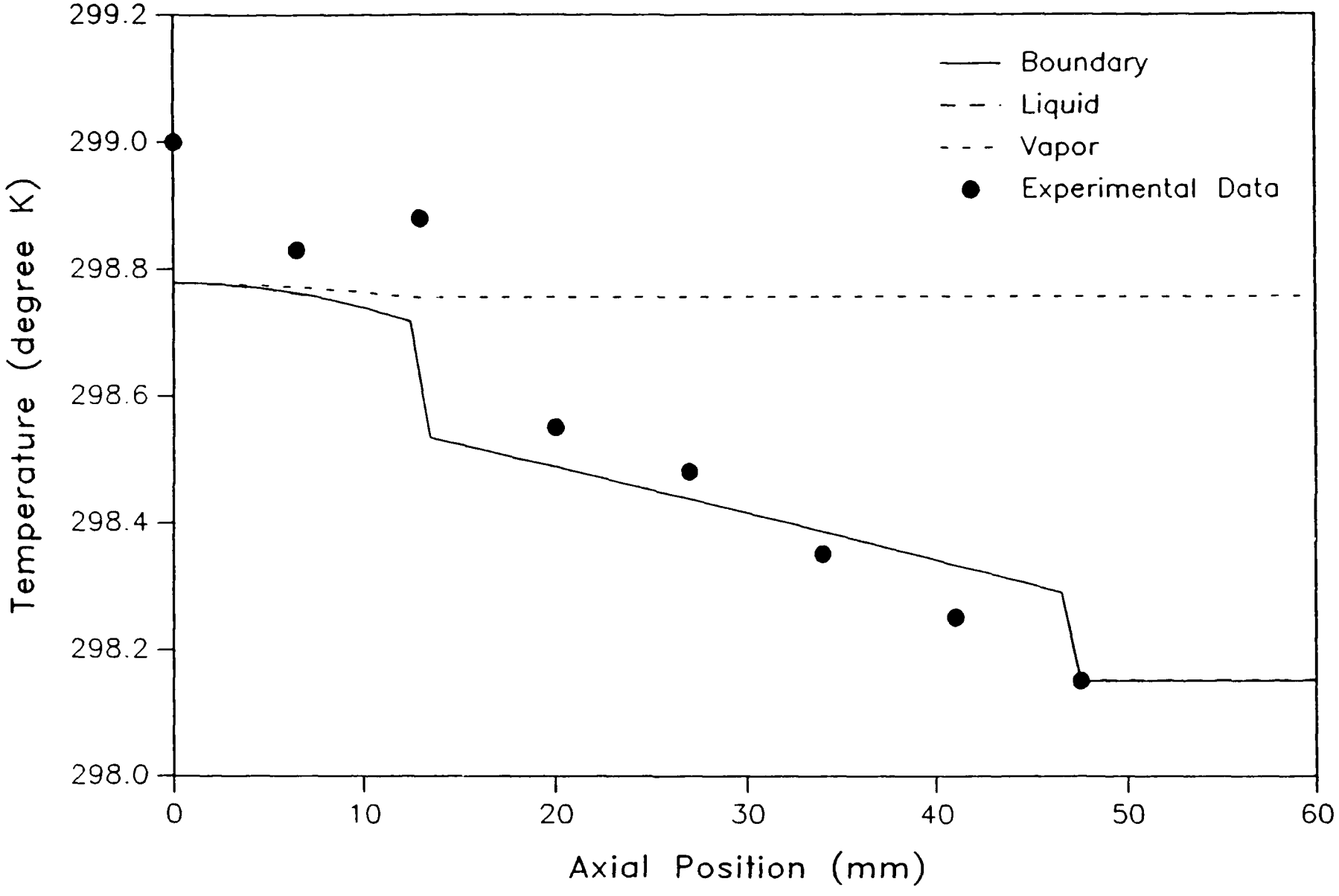


**Fig. 15 Comparison of predicted and measured boundary temperature distribution, (Power 0.12 W, $T_c$ 24.5°C, no tilt).**

as predicted by the numerical model for a power level of 0.12 W. As illustrated, the temperature data closely follow the predicted trend. Some heat rejection occurrs in the adiabatic section, however, the condenser temperature remains relatively constant. Throughout the entire length, however, the predicted and measured temperature distributions are extremely close to the predicted value, with the largest deviation being less than 0.3°C. Figure 16 compares the predicted and the measured temperature difference between the evaporator, Thermocouple 1, and the condenser, Thermocouple 9, as a function of time for a power input of 0.12 W and at a horizontal position. As illustrated, the final steady-state temperature difference between the evaporator and the condenser as predicted by the model is within 12% of the measured value. The numerical model, however, predicts a much more rapid startup of the heat pipe than that obtained experimentally. This predicted rapid startup may be the result of the inherent shortcomings of the model, while in the actual case heat is rejected from the evaporator portion of the heat pipe through vaporization of the liquid, it is also rejected through conduction to the support member and radiation to the surroundings. In addition, the numerical model assumes instantaneous heat addition while in the experimental case, some sensible heat is absorbed by the mass of the heater wires, the heater, and the lead wires. The small dip in the theoretical predicted temperature difference occurring at approximately 10 seconds into the test is the result of the reverse liquid flow discussed previously. As shown, the experimental results indicate no such reverse flow. This may be the result of the reduced time constant caused by the mass of heat pipe case material.

Figure 17 illustrates a similar comparision at a tilt angle of 15 degrees (evaporator down). As shown, for this case, the numerical model does not predict any reverse liquid flow and significantly underestimates the

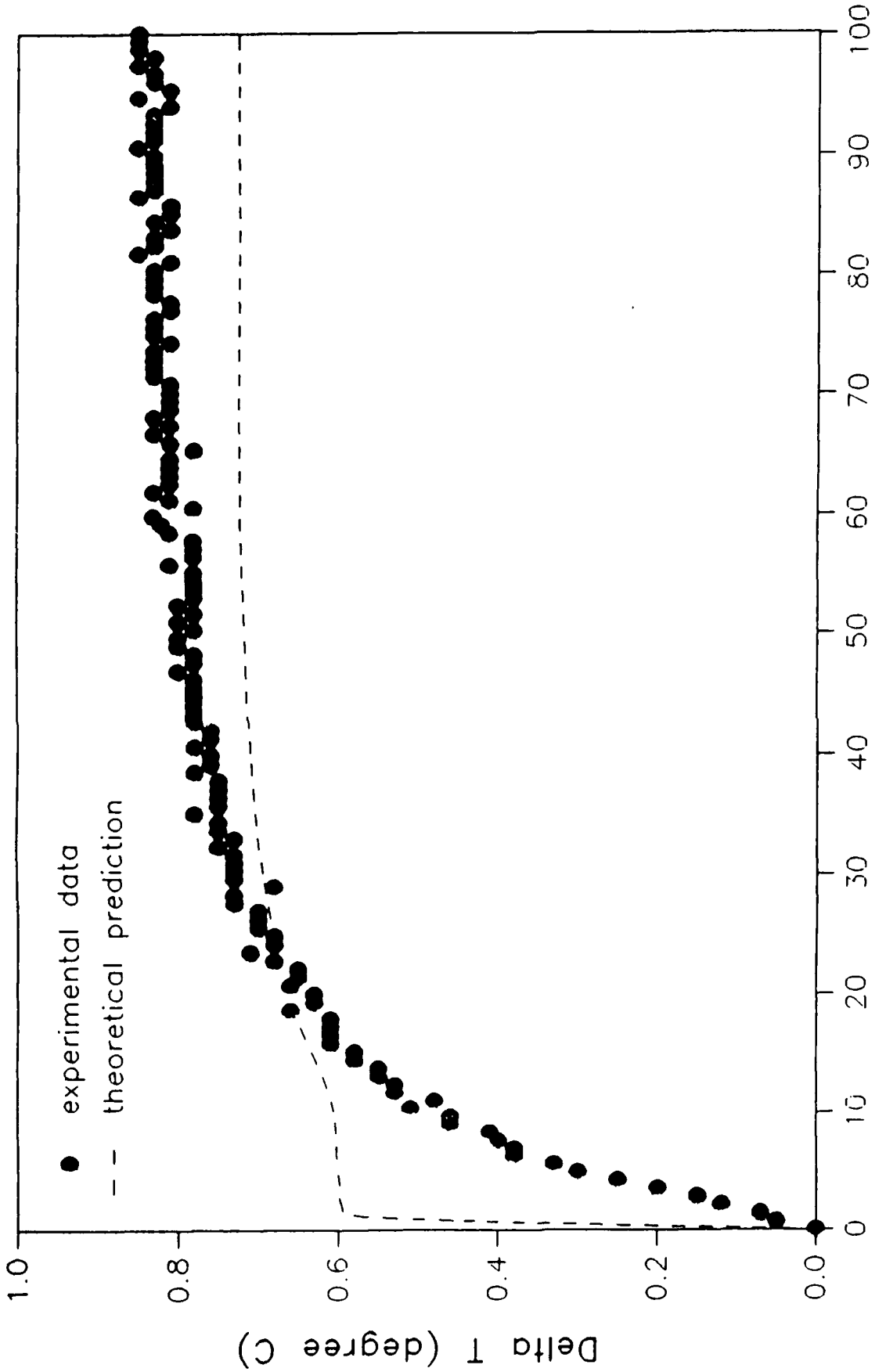


**Fig. 16 Comparison of predicted and measured evaporator temperature difference as a function of time, (Power 0.12 W, $T_c$ 24.5°C, evaporator down).**

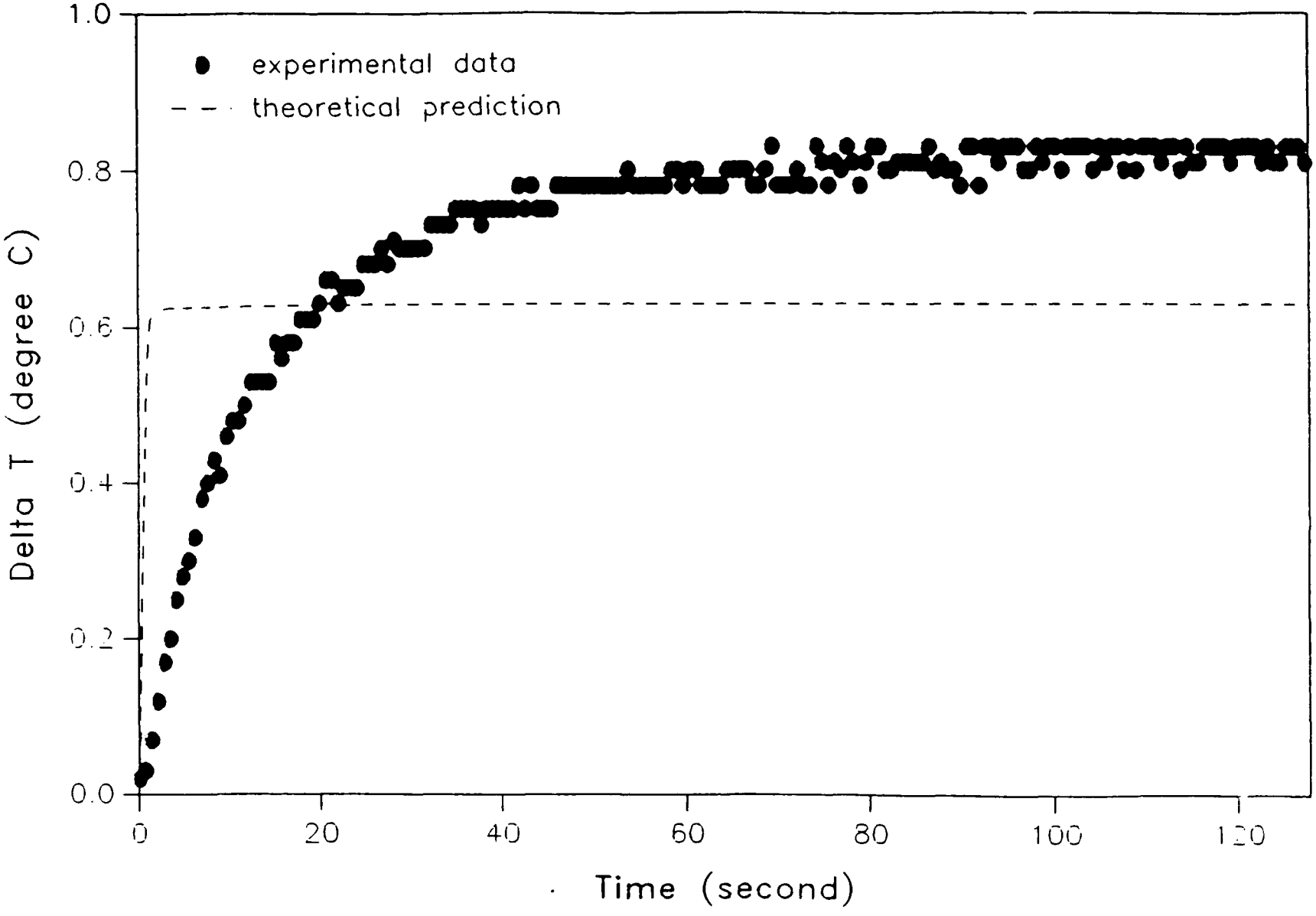


**Fig. 17 Comparison of predicted and measured evaporator temperature difference as a function of time, (Power 0.12 W, $T_c$ 24.5°C, no tilt).**

longitudinal temperature difference. Again, the disparity between the measured and predicted values is believed to be due to differences in the numerical model and the actual experimental tests. In the numerical model, the effects of the end wall of the heat pipe were not incorporated. This end region provides an additional capilllary radius which helps retain liquid in the evaporator region of the heat pipe and results in higher power levels prior to the onset of dryout. These increased power levels manifest themselves as an increase in temperature differences, similar to that shown in Fig. 17.

## 4.0 SUMMARY

An investigation to develop a numerical model capable of predicting the transient performance, determining the effect of variations in the size and optimizing the cross-sectional shape of a tapered micro heat pipe has been conducted. Several heat pipes which utilize the optimized shape were evaluated experimentally to determine their suitability for heat removal from a ceramic chip carrier and to provide data through which the numerical model could be validated. The numerical model was found to be capable of accurately predicting the maximum transport capacity prior to the onset of dryout, the temperature distribution throughout the longitudinal position, and the temperature difference between different locations on the heat pipe to within 0.3°C prior to the onset of dryout. In addition, the transient model predicted the operation and temperature distribution of the tapered micro heat pipe to within ±12 % over a wide range of powers and operating temperatures.

As a result of this effort, the numerical model can be confidently used to identify, evaluate, and better understand the phenomena that governs the transient behavior of micro heat pipes as a function of the physical shape, properties of the working fluid, and principal dimensions.

## REFERENCES


1 Peterson, G. P. and Ortega, A., "Thermal Control of Electronic Equipment and Devices," in Advances in Heat Transfer, (J. Hartnett and T. Irvine, eds.), Pergamon Press, pp. 181-314, 1990.

2 Cotter, T. P., "Principles and Prospects of Micro Heat Pipes," Proc. 5th Int'l. Heat Pipe Conf., Tsukuba, Japan, pp. 328-335, 1984.

3 Peterson, G. P., Weichold, M. H. and Mallik, A., U.S. Patent Pending, Patent Application no. 380,189, U.S. Patent and Trademark Office, Filed on July 14, 1989.

4 Babin, B. R., Peterson, G. P. and Wu, D., "Analysis and Testing of a Micro Heat Pipe During Steady-State Operation," 1989 ASME National Heat Transfer Conf., Paper No. ASME 89-HT-17, Philadelphia, PA, August 1989.

5 Chi, S. W., Heat Pipe Theory and Practice, McGraw-Hill Publishing Company, New York, 1976.

6 Dunn, P. D. and Reay, D. A., Heat Pipes, 3rd edition, Pergamon Press, New York, 1982.

7 Collier, J. G., Convective Boiling and Condensation, McGraw-Hill Book Co. New York, NY, 1981.

8 Colwell, G. T. and Chang, W. S., "Measurements of the Transient Behavior of a Capillary Structure Under Heavy Thermal Loading," Int'l J. of Heat and Mass Transfer, Vol. 27, No. 4, pp. 541-551, 1984.

9 Peterson, G. P., Babin, B.R. and Wu, D., "Analytical and Experimental Investigation of Miniature Heat Pipes," Wright-Patterson Rpt. no. WRDC-TR-89-2067, Wright Research and Development Center, Wright-Patterson, Ohio. 1989.

10 Peterson, G. P., "Capillary Priming Characteristics of a High Capacity Dual Passage Heat Pipe," Chemical Engineering Communications, Vol. 27, No.1, pp. 119-126, 1984.




☆U.S.Government Printing Office: 1990—748-056/24407